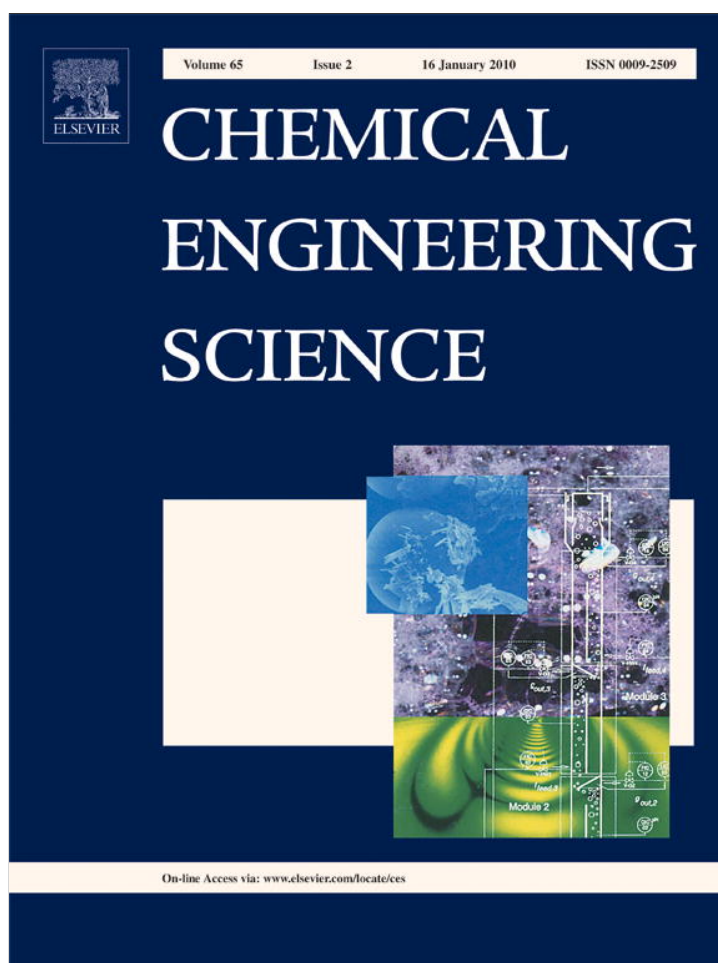


Provided for non-commercial research and education use.
Not for reproduction, distribution or commercial use.

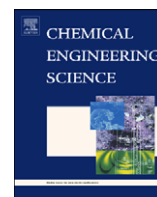


This article appeared in a journal published by Elsevier. The attached copy is furnished to the author for internal non-commercial research and education use, including for instruction at the authors institution and sharing with colleagues.

Other uses, including reproduction and distribution, or selling or licensing copies, or posting to personal, institutional or third party websites are prohibited.

In most cases authors are permitted to post their version of the article (e.g. in Word or Tex form) to their personal website or institutional repository. Authors requiring further information regarding Elsevier's archiving and manuscript policies are encouraged to visit:

<http://www.elsevier.com/copyright>



Modeling of transport and chemistry in channel flows of automotive catalytic converters

N. Mladenov, J. Koop, S. Tischer, O. Deutschmann*

Institute for Chemical Technology and Polymer Chemistry, Universität Karlsruhe (TH), Karlsruhe Institute of Technology (KIT), 76128 Karlsruhe, Germany

ARTICLE INFO

Article history:

Received 2 February 2009

Received in revised form

31 August 2009

Accepted 14 September 2009

Available online 26 September 2009

Keywords:

Catalysis

Modeling

Mass-transfer

Exhaust-gas cleaning

Pt

Numerical simulation

Washcoat

ABSTRACT

A novel comprehensive numerical study is presented for a better understanding of mass transfer in channel flows with catalytically active walls at moderate temperatures and surface reaction rates. Altogether, 18 different numerical models are compared, which represent mass transfer in single channels of a honeycomb-type automotive catalytic converter operated under direct oxidation conditions. Three different channel geometries have been investigated: circular cross-section, square cross-section, and square cross-section with rounded corners (fillets). 1D plug-flow, 2D boundary-layer and Navier–Stokes, and 3D Navier–Stokes equations are applied to model the reactor geometry. The diffusion limitation within the porous washcoat has been modeled by a simplified zero-dimensional effectiveness factor model as well as multidimensional reaction–diffusion models. Furthermore, simulations are also carried out for cases with instantaneous diffusion within the washcoat. All numerical models account for the coupled interactions of mass-transfer and heterogeneous chemistry within the channels. The chemical conversion of the pollutants on the platinum catalyst is described by an elementary-step-like heterogeneous reaction mechanism consisting of 74 reactions among 11 gas-phase species and 22 adsorbed surface species. The results of numerical simulations are compared with experimental data.

© 2009 Elsevier Ltd. All rights reserved.

1. Introduction

Tremendous reduction of hydrocarbons, carbon monoxide and nitric oxides emitted from internal combustion engines is today achieved by the application of automotive catalytic converters. They commonly consist of monolithic structures of many parallel channels (honeycomb-type catalysts), each of which is coated with a porous material (washcoat). This porous material is usually alumina and has the objective of increasing the catalytic active surface area. The catalytic reactions take place on noble metal particles distributed in the washcoat.

The noble metal catalysts platinum, palladium, and rhodium guarantee high conversion but also significantly contribute to high production costs of the automobile exhaust-gas after-treatment system; those costs are meanwhile on the order of the costs of the engine itself. Reduction of the amount of noble metal content without sacrificing performance demands a detailed understanding of the complex processes in the converter under varying operating conditions, i.e. exhaust gas compositions, flow rate, and temperature. Design and optimization of a catalytic converter is challenging due to the complex interaction between chemical

reactions and mass and heat transfer. Experimental test bench measurements are finally needed but they also are expensive and time-consuming and, therefore, should be limited. Furthermore, those experiments are difficult to be interpreted concerning the details of the different chemical and physical processes inside the honeycomb structure.

Here, reliable numerical simulations can serve as a powerful method to investigate and eventually optimize the performance of catalytic converters. Understanding the temperature and species profiles inside the converter is an important step in the development of highly optimized catalytic systems and is subject of many publications. Various numerical models with different complexity were developed. Baba et al. (1996), Chatterjee et al. (2002), Tischer et al. (2003) and Jahn et al. (1997) simulated the transient behavior of the entire monolithic converter. Other authors assume that, under certain operating conditions, all channels behave essentially alike and analyze a single channel. This approach allows a more detailed insight into the transport phenomena and chemical reactions within the channel. Raja et al. (2000) compared various simplified 1D- and 2D-formulations of the steady-state Navier–Stokes equations for catalytic combustion of methane in a cylindrical channel. Chatterjee (2001) and Chatterjee et al. (2001) developed detailed surface reaction mechanisms, using 1D- and 2D-channel models including simplified and detailed reaction–diffusion models for the washcoat.

* Corresponding author.

E-mail address: deutschmann@kit.edu (O. Deutschmann).

Deutschmann et al. (2001) introduced a three-dimensional single-channel model to investigate the natural gas conversion in monolithic converters, using a set of one-dimensional reaction–diffusion equations to calculate the species concentrations and surface coverages inside the washcoat. Tuttlies et al. (2004) applied a simplified shrinking core-type model coupled with a discretized 1D monolith channel model to simulate the transient NO_x storage along the channel length. Canu and Vecchi (2002) compared 2D and 3D single channel models to predict ignition temperatures applying a global kinetic equation for the methane/air heterogeneous combustion on Pt. Maestri et al. (2008) and Appel et al. (2002) developed two-dimensional channel models coupling surface and gas-phase reactions to investigate the hydrogen combustion over Pt and Rh/ Al_2O_3 . Ramanathan et al. (2004) studied the geometry effects on ignition for fully developed laminar flow in various channel geometries using a 3D convection–diffusion model. Groppi and Tronconi (1997) introduced 1D and 3D models to investigate the steady-state mass and heat transfer in equilateral triangular channels. Leung et al. (1996) applied a 2D finite element model to investigate the impact of diffusion on the reaction rate in the washcoat of a catalytic monolith reactor. An axisymmetric model to investigate the effect of washcoat thickness on the reforming performance of a monolithic converter was proposed by Stutz and Poulidakos (2007). Single channel simulations carried out by Hayes et al. (2004), Holmgren and Andersson (1998), and Wanker et al. (2000) took the mass-transfer effects in the washcoat into account. Altogether, a variety of monolithic structured catalysts for different applications have been studied over the years, which applied varying models for the flow field and catalytic chemistry. However, only few investigations systematically studied the impact of mass transport (convection and diffusion) on the model predictions. Such case studies may be grouped into systems with very fast reaction rates such as catalytic combustion (Raja et al. 2000) and systems with relatively slow rates such as automotive catalytic converters. The consequences of the interaction of chemistry and mass/heat transport of course differ in both systems. Here, we focus on conversion in automotive catalytic converters exhibiting a relatively slow reaction rate, i.e., full conversion is achieved over a catalyst length of centimeters rather than millimeters such as in short-contact time reactors (Raja et al., 2000; Deutschmann and Schmidt, 1998).

The current paper has the objective to evaluate the role of mass transport in automotive catalytic converters using four different simplified formulations of the Navier–Stokes equations for steady-state isothermal flows. For this purpose, a single channel of honeycomb-type catalyst was modeled, whereas three different channel geometries were used—cylindrical channel, a channel with square cross-section and a square channel with rounded corners (fillets). The conversions predicted by the applied one-, two- and three-dimensional channel models are compared with each other. Additionally, infinitely fast, simplified and detailed diffusion models are applied to account for the influence of the washcoat on the conversion of the species of interest. We use a direct oxidation catalyst (DOC) as example, which is usually operated under lean (in excess of oxygen) conditions. The pollutants here are unburnt and not completely burnt hydrocarbons (HC), carbon monoxide (CO), and nitrogen oxides (NO and NO_2). The hydrocarbons are commonly represented by propylene (C_3H_6). The conclusions drawn from the present study, however, can also be applied for three-way catalysts and even other catalytic systems with similar structure (channel-like) and operating conditions (temperature, relatively low reaction rate).

All approaches of this study to model mass transfer include a detailed surface reaction mechanism (Koop and Deutschmann, 2009) developed for Pt-catalyzed abatement of pollutant

emissions from internal combustion engines operated at lean conditions. The computed conversions of pollutants are compared with experimental data taken from Schmeißer et al. (2007), who investigated the NO_x storage-reduction catalysts. In our study, results from the steady-state lean-phase experiments without storage component are used only to show the general applicability of the models. The objective of our paper is the evaluation of transport models and not the reproduction of experimental data, the mechanism used has already been evaluated in a recent paper (Koop and Deutschmann, 2009).

2. Modeling approach

2.1. General model assumption

In this study, a comparison of one-, two- and three-dimensional single channel models under isothermal, steady-state operating conditions is presented. Depending on the complexity of the implemented model, the computational time can vary from few seconds to several days. The simple one-dimensional plug-flow model neglects the impact of the diffusion on the reacting flow. A differential–algebraic-equation (DAE) initial-value problem has to be solved, which describes the species concentrations as a function of the axial position in the channel. In order to improve the accuracy of the plug-flow model, mass-transfer coefficients are also included. Based on empirical dependencies, they account for the transport limitation between the gas composition in the channel and at the reacting channel surface, forming an additional set of non-linear algebraic equations. For the solution of the two-dimensional case, two models are applied: the first one, based on the boundary-layer equations (Schlichting, 1968; Kee et al., 2003) and the second one, based on the 2D Navier–Stokes equations. The boundary-layer model considers only radial diffusion to and from the wall, whereas the Navier–Stokes equations take both axial and radial mass and momentum transport into account. The one- and two-dimensional models consider cylindrical channel geometry. The three-dimensional simulations handle a channel with square cross-section and a square channel with fillets. The latter geometry is typical for washcoated monolithic converters. The three-dimensional models are solved by means of complete Navier–Stokes equations. The effect of diffusion inside the washcoat on the conversion rate is also included in the present study. For this purpose, a simplified effectiveness coefficient-factor model and detailed reaction–diffusion models are applied and compared to calculations with infinitely fast mass transport within the washcoat. The diffusion coefficients in the porous media are determined based on the Bosanquet formula (Hayes and Kolaczkowski, 1997). In this approach, an equivalent Fick diffusion coefficient is defined as a combination of the mixture and Knudsen diffusion coefficients.

In the cases studied, the gas-mixture enters the reactive channel with uniform inlet velocity. The non-cylindrical channels have the same catalyst loading and cross-section as the cylindrical, which results in identical mass fluxes through all modeled channels. Ideal-gas behavior and laminar flow conditions are assumed. Furthermore, the energy balance is excluded from all simulations in order to compare the results with the isothermal experiments described in Section 3.1.

2.2. Modeling flow in catalytic channels

2.2.1. Three-dimensional Navier–Stokes equations

Three-dimensional Navier–Stokes equations represent the most adequate description of reacting flow with arbitrary

geometries. They form a set of elliptical equations for the conservation of total mass, momentum in x , y , and z direction, mass of the single species and energy (not considered here), providing solution for the velocity, pressure, temperature, and species concentration fields inside the flow domain. In the current study, they are used to model the channels with non-circular cross-section. Due to the symmetry properties of these channels, only an eighth of their structure is modeled. The Navier–Stokes equations to be solved for a steady-state laminar problem are:

Conservation of total mass

$$\nabla \cdot (\rho \vec{v}) = 0 \quad (1)$$

Conservation of momentum

$$\nabla \cdot (\rho \vec{v} \otimes \vec{v}) = \vec{F} - \nabla p + \nabla \cdot \left[\mu \left(\nabla \vec{v} + (\nabla \vec{v})^T - \frac{2}{3} (\nabla \cdot \vec{v}) \mathbf{I} \right) \right] \quad (2)$$

Conservation of species mass

$$\nabla \cdot (\rho \vec{v} Y_i) = - \nabla \cdot \vec{J}_i + \dot{\omega}_i W_i, i = 1, \dots, N_g \quad (3)$$

The ideal-gas law provides an additional equation for the pressure:

$$p = \frac{\rho RT}{W} \quad (4)$$

In the above equations, time-dependent terms are omitted. The dependent variables are the velocity $\vec{v} = (u, v, w)$, the species mass fractions Y_i , and pressure p . The variables ρ and μ are mass density and dynamic viscosity, respectively, \vec{J}_i denotes the diffusive mass flux. Ignoring thermal diffusion, its spatial components in the channel can be written as:

$$\vec{J}_i = - \rho \frac{W_i}{W} D_{M,i} \nabla X_i \quad (5)$$

Here, $D_{M,i}$ is the mixture diffusion coefficient between the i th species and the remaining mixture and X_i the mole fraction of species i . W is the molecular weight of the gas-mixture and W_i is the molecular weight of the i th species. The body force \vec{F} as well as the homogeneous reaction source term for gas-phase species $\dot{\omega}_i$ are not taken into account in the current study.

2.2.2. Two-dimensional Navier–Stokes equations

Here, the 2D Navier–Stokes equations are used to simulate reacting flows in cylindrical channels. Due to the rotational symmetry of geometry, boundary conditions and body forces, the three independent variables of the common Navier–Stokes problem are reduced to two: axial coordinate z and radial coordinate r . Thus, the computational time could be significantly reduced.

Conservation of total mass

$$\frac{\partial(\rho w)}{\partial z} + \frac{1}{r} \frac{\partial(r \rho v)}{\partial r} = 0 \quad (6)$$

Conservation of axial momentum

$$\rho \left(w \frac{\partial w}{\partial z} + v \frac{\partial w}{\partial r} \right) = - \frac{\partial p}{\partial z} + \frac{\partial}{\partial z} \left[2\mu \frac{\partial w}{\partial z} - \frac{2}{3} \mu \left(\frac{\partial w}{\partial z} + \frac{1}{r} \frac{\partial r v}{\partial r} \right) \right] + \frac{1}{r} \frac{\partial}{\partial r} \left[\mu r \left(\frac{\partial v}{\partial z} + \frac{\partial w}{\partial r} \right) \right] \quad (7)$$

Conservation of radial momentum

$$\rho \left(w \frac{\partial v}{\partial z} + v \frac{\partial v}{\partial r} \right) = - \frac{\partial p}{\partial r} + \frac{\partial}{\partial z} \left[\mu \left(\frac{\partial v}{\partial z} + \frac{\partial w}{\partial r} \right) \right] + \frac{\partial}{\partial r} \left[2\mu \frac{\partial v}{\partial r} - \frac{2}{3} \mu \left(\frac{\partial w}{\partial z} + \frac{1}{r} \frac{\partial r v}{\partial r} \right) \right] + \frac{2\mu}{r} \left(\frac{\partial v}{\partial r} - \frac{v}{r} \right) \quad (8)$$

Conservation of species mass

$$\rho \left(w \frac{\partial Y_i}{\partial z} + v \frac{\partial Y_i}{\partial r} \right) = - \frac{\partial J_{i,z}}{\partial z} - \frac{1}{r} \frac{\partial (r J_{i,r})}{\partial r} \quad (9)$$

In the above equations, v denotes the velocity in radial direction and w in axial direction. The spatial components of the diffusive mass flux are given by:

$$J_{i,z} = - \rho \frac{W_i}{W} D_{M,i} \frac{\partial X_i}{\partial z}, \quad J_{i,r} = - \rho \frac{W_i}{W} D_{M,i} \frac{\partial X_i}{\partial r} \quad (10)$$

2.2.3. Two-dimensional boundary-layer equations

At the beginning of the 20th century, Prandtl introduced the boundary-layer theory—approximation of the Navier–Stokes equations widely spread in fluid mechanics. At high flow rates in a channel, radial diffusion and convective transport prevail over axial diffusion. Accordingly, all second derivatives in z direction as well as the axial diffusion term $J_{i,z}$ can be eliminated. Furthermore, pressure gradients in radial direction also vanish (Eq. (13)). The original system of elliptical differential equations is reduced to a parabolic one, with the axial coordinate z representing the time-like coordinate. Thus, the boundary-layer approximation enables a downstream solution of the reacting flow problem in a single sweep of integration using an adaptive step size.

Conservation of total mass

$$\frac{\partial(\rho w)}{\partial z} + \frac{1}{r} \frac{\partial(r \rho v)}{\partial r} = 0 \quad (11)$$

Conservation of axial momentum

$$\rho \left(w \frac{\partial w}{\partial z} + v \frac{\partial w}{\partial r} \right) = - \frac{\partial p}{\partial z} + \frac{1}{r} \frac{\partial}{\partial r} \left(\mu r \frac{\partial w}{\partial r} \right) \quad (12)$$

Conservation of radial momentum

$$0 = \frac{\partial p}{\partial r} \quad (13)$$

Conservation of species mass

$$\rho \left(w \frac{\partial Y_i}{\partial z} + v \frac{\partial Y_i}{\partial r} \right) = - \frac{1}{r} \frac{\partial (r J_{i,r})}{\partial r} \quad (14)$$

Raja et al. (2000) showed that for sufficiently high Re (> 20) numbers in the catalytically coated channel, boundary-layer approximations are in good agreement with Navier–Stokes solutions at high temperature and fast reaction rates. Even though the Re numbers in the cases studied here are higher, the flow is still laminar, however, the reaction rates and temperature are much lower.

2.2.4. One-dimensional plug-flow equations

Plug-flow equations represent a simplification of the boundary-layer model assuming negligible axial diffusion and instantaneous diffusion in radial direction. Thus, all variables become radially independent and are expressed as functions of only the axial position z in the channel. For a cylindrical channel, the conservation equations can be written in the following form:

Conservation of total mass

$$\frac{\partial(\rho w)}{\partial z} = \frac{2}{r_{\text{channel}}} \sum_{\text{gas}} F_{\text{cat/geo}} W_i \dot{s}_i \quad (15)$$

Conservation of momentum

$$\rho w \frac{\partial w}{\partial z} + \frac{2w}{r_{\text{channel}}} \sum_{\text{gas}} F_{\text{cat/geo}} W_i \dot{s}_i = - \frac{\partial p}{\partial z} + \frac{\rho w^2}{r_{\text{channel}}} \frac{16}{Re} \quad (16)$$

Conservation of species mass

$$\rho w \frac{\partial Y_i}{\partial z} + \frac{2Y_i}{r_{\text{channel}}} \sum_{\text{gas}} F_{\text{cat/geo}} W_i \dot{s}_i = \frac{2F_{\text{cat/geo}} W_i \dot{s}_i}{r_{\text{channel}}}, i = 1, \dots, N_g \quad (17)$$

where r_{channel} is the channel radius and $F_{\text{cat/geo}}W_i\dot{s}_i$ is the mass source term for the i th gas species as a result of surface reactions. The surface scaling factor $F_{\text{cat/geo}}$ represents the area ratio of the catalytic active surface in the washcoat to the channel geometrical surface. The right side of Eq. (15) and the second left terms in Eqs. (16) and (17) describe the net mass addition (or depletion) from the gas flow by surface reaction such as chemical vapor deposition (CVD). In the present study, we model steady-state heterogeneous catalytic reactions without mass ablation or deposition, hence we assume zero net mass exchange and eliminate this term.

Raja et al. (2000) derived following expression for the validity of the plug-flow model:

$$\frac{d}{L} < Re Sc < \frac{L}{d} \quad (18)$$

where $d = 1$ mm is the diameter of the channel, $L = 20$ cm is the channel length and Sc is the Schmidt number. Accordingly, the condition $0.005 < Re Sc < 200$ must be fulfilled. At lean operating conditions $Sc \approx 1$ for most species. As will be shown in Section 3.2, the Re numbers of our system amount to 177 and 201. Due to the similarities with the current problem, the plug-flow model was considered as well.

2.2.5. One-dimensional plug-flow model with mass-transfer coefficients

This enhanced model aims to improve the accuracy of the general plug-flow formulation. Mass-transfer coefficients (MTC) are introduced to account for the species transport limitation between the averaged gas-mixture and the gas-mixture at the catalytic active channel surface. They are defined by the following expression:

$$h_i = \frac{J_{i,r}}{\rho_s Y_{i,s} - \bar{\rho} \bar{Y}_i} \quad (19)$$

Here, h_i is the species mass-transfer coefficient, $J_{i,r}$ the radial component of the species mass flux at the channel wall, ρ_s the density of the gas-mixture at the channel surface and $Y_{i,s}$ the mass fraction of species i at the channel surface. The variables $\bar{\rho}$ and \bar{Y}_i stand for the averaged density and species mass fraction as defined in Eqs. (20) and (21).

$$\bar{\rho} = \frac{\int_0^A \rho dA}{\int_0^A dA} \quad (20)$$

$$\bar{Y}_i = \frac{\int_0^A \rho u Y_i dA}{\int_0^A \rho u dA} \quad (21)$$

Here, A represents the surface area of the channel cross-section. Hence, the variable $Y_{i,s}$ is expressed by means of the surface reaction rate \dot{s}_i :

$$h_i(\rho_s Y_{i,s} - \bar{\rho} \bar{Y}_i) = F_{\text{cat/geo}} W_i \dot{s}_i, \quad i = 1, \dots, N_g. \quad (22)$$

Eq. (22) forms a nonlinear algebraic equation system which has to be solved simultaneously with the differential equations (15)–(17), whereas $Y_{i,s}$ is used instead of Y_i for the calculation of \dot{s}_i . The mass-transfer coefficient h_i is a function of the Sherwood number:

$$h_i = \frac{Sh_i D_{M,i}}{d} \quad (23)$$

The variable $D_{M,i}$ represents the molecular diffusion coefficient. The Sherwood number used here is based on the following empirical correlation (Hayes and Kolaczkowski, 1997):

$$Sh_i = 3.675 + 8.827 \left(\frac{1000}{Gz_i} \right)^{-0.545} e^{-48.2/Gz_i} \quad (24)$$

where Gz_i is the dimensionless Graetz number:

$$Gz_i = \frac{z D_i^M}{d^2 w} \quad (25)$$

2.3. Modeling diffusion and reactions in the washcoat

Monolithic catalysts are commonly coated with a 10–100 μm thick porous layer made out of, e.g., alumina to enlarge the surface-to-volume ratio. In this so-called washcoat, reactants and products diffuse from/to the open fluid phase through nano and micro pores to/from the noble metal particles being 1–1000 nm in size, on which the catalytic conversion occurs. Finite species diffusion fluxes combined with chemical reactions may lead to concentration gradients within the washcoat, i.e. spatially varying reaction rates. Consequently, finite species diffusion may slow down the overall conversion observed. Several models have been developed to account for this transport limitation effect.

2.3.1. Modeling instantaneous diffusion

This model eliminates the impact of the parameters washcoat thickness, porosity, pore, and particle diameters. Thus, the influence of mass transport limitation on conversion in the washcoat is neglected corresponding to a channel in which the catalyst is virtually distributed on the gas-phase/washcoat interface.

A boundary condition defined at the gas-phase/washcoat interface is that the velocity components tangential to the interface vanish (i.e. w in the 2D case). A further boundary condition considers the molar production of species i due to heterogeneous chemical reactions \dot{s}_i . It implies that the gas-phase species mass flux produced by chemical reactions at the gas-phase/washcoat interface must correspond to the diffusive flux of the species in the gas:

$$F_{\text{cat/geo}} W_i \dot{s}_i = - (J_{i,r} + \rho Y_{i,s} v_{st}), \quad i = 1, \dots, N_g \quad (26)$$

Eq. (26) provides solution for the gas-phase species mass fractions $Y_{i,s}$ at the surface (2D case). In the case of non-cylindrical channel geometries, $J_{i,r}$ has to be replaced by the J -component normal to the wall. The product $F_{\text{cat/geo}} W_i \dot{s}_i$ represents the chemical source term, in which \dot{s}_i is the computed molar reaction rate by catalytic reactions computed using the gas-phase concentrations at the fluid–washcoat interface. The Stefan-velocity v_{st} is normal to the channel surface and accounts for the net mass exchange at the wall. For our steady-state with catalytic heterogeneous reactions, this velocity vanishes.

2.3.2.1. General reaction–diffusion model in multidimensional porous structures. Species mass transfer in porous media can be modeled by adding momentum source terms to Eqs. (2) or (9) and (10) for the 3D and the 2D cases, respectively. These source terms cause a pressure drop proportional to the fluid velocity in the particular direction. In our case, we treat the washcoat as homogeneous isotropic porous media. Under this assumption, the source terms can be given as

$$\vec{S} = - \left(\frac{\mu}{\alpha} + \frac{\rho C_2 |\vec{v}|}{2} \right) \vec{v} \quad (27)$$

which is based on Forchheimer's modified formulation of Darcy's law (Fluent). Here, μ is the dynamic viscosity, α the permeability, and C_2 the inertial resistance factor. The first term in the brackets of Eq. (27) represents viscous loss and the second inertial loss.

The permeability and the inertial resistance factor can be derived from Ergun's formula for a packed bed reactor:

$$\alpha = \frac{d_m^2}{150} \frac{\varepsilon^3}{(1 - \varepsilon)^2} \quad (28)$$

and

$$C_2 = \frac{3.5(1 - \varepsilon)}{d_m \varepsilon^3} \quad (29)$$

where ε is the porosity and d_m the mean particle diameter.

Mass fluxes in the porous media are calculated similarly to Eqs. (5) and (10), whereas the mixture diffusion coefficient $D_{M,i}$ is replaced by an equivalent Fick diffusion coefficient $D_{eff,i}$ taking both mixture and Knudsen diffusion into account:

$$\frac{1}{D_{eff,i}} = \frac{\tau}{\varepsilon} \left(\frac{1}{D_{M,i}} + \frac{1}{D_{knud,i}} \right) \quad (30)$$

The empirical variable tortuosity τ represents the deviation of the washcoat pores from the ideal cylinder. The Knudsen diffusion coefficient for the i th species is given by:

$$D_{knud,i} = \frac{d_p}{3} \sqrt{\frac{8RT}{\pi W_i}} \quad (31)$$

Here, R is the gas constant and T the temperature.

In contrast to Section 2.3.1, the catalytic source term does not appear as a boundary condition but as a volumetric mass source term $W_i \gamma \dot{s}_i$ on the right-hand side of species' continuity Eqs. (3) and (9). The variable $\gamma = F_{cat}/t_w$ stands for the catalyst density (active surface per washcoat volume), where t_w is the washcoat thickness.

2.3.2.2. Washcoat modeling by 1D reaction–diffusion equation. In the present study, we also used 1D reaction–diffusion equations to describe species concentration profiles inside the washcoat coupled with the boundary-layer equations. The species gradients in the washcoat directly affect the local surface reaction rates \dot{s}_i (Hayes and Kolaczkowski, 1997). The assumption that the axial concentration gradients are considerably lower compared to the radial gradients allows the one-dimensional discretization of the problem. Hence, the reaction–diffusion equation can be expressed as

$$\frac{\partial \bar{J}_{i,r}^w}{\partial r} - \gamma \dot{s}_i = 0 \quad (32)$$

$$\bar{J}_{i,r}^w = -D_{eff,i} \frac{\partial c_{w,i}}{\partial r} \quad (33)$$

Here, $\bar{J}_{i,r}^w$ is the radial diffusion molar flux, $c_{w,i}$ the molar concentration and $D_{eff,i}$ the effective Fick coefficient (Eq. (30)) of species i in the washcoat. The radial diffusion flux at the gas-phase/washcoat interface is treated as an effective surface reaction rate: $\dot{s}_{eff,i} = \bar{J}_{i,r}^w(r = d/2)$. In order to close the equation system (32), two boundary equations are required:

$$c_{i,w}(r = d/2) = c_{0,i}; \quad \frac{\partial c_{i,w}(r = d/2 + t_w)}{\partial r} = 0 \quad (34)$$

The first boundary condition implies that the concentration at the gas-phase/washcoat interface is the given concentration in the gas-phase. The second one assumes that the washcoat is thick enough and concentration gradients vanish at the washcoat/support boundary.

2.3.2.3. Washcoat modeling using effectiveness factor approach. The reaction–diffusion Eq. (32) for a single species can be solved analytically if the following two conditions are fulfilled:

- The species is consumed and the reaction rate is proportional to the concentration ($\dot{s} = -k \cdot c$, k is the rate constant).
- The diffusion coefficient is constant.

The effective surface reaction rate then becomes

$$\dot{s}_{eff} = -D_{eff} \lambda c_0 \tanh(\lambda t_w), \quad \text{with } \lambda = \sqrt{\frac{\gamma k}{D_{eff}}} \quad (35)$$

Assuming no diffusion limitation, we obtain the following maximum reaction rate

$$\dot{s}_{max} = -F_{cat}/t_w k c_0 = -\gamma t_w k c_0 \quad (36)$$

The effectiveness factor η is defined as the ratio of the effective to the maximum reaction rate:

$$\eta = \frac{\dot{s}_{eff}}{\dot{s}_{max}} = \frac{\tanh(\lambda t_w)}{\lambda t_w} \quad (37)$$

whereas the dimensionless term λt_w is also known as Thiele modulus. In order to extend this approach for multi-species systems, one species that satisfies the above prerequisites has to be chosen. This species must be representative for the behavior of the whole system. Its effectiveness factor η is then computed and multiplied with the reaction rates of all species, thus providing the required effective steady-state reaction rates at the washcoat–gas-phase boundary:

$$\dot{s}_{eff,i} = \eta \dot{s}_i \quad (38)$$

The resulting diffusion model is zero-dimensional, a huge simplification compared to the reaction–diffusion model. NO is the species determining the NO-oxidation at lean-burn operating conditions. Hence, the effectiveness factor for NO was used for the calculations in the current paper. This assumption is a strong simplification because in complex reaction networks, diffusion of a single species may not be rate-limiting, depending of the position in the reactor different diffusions processes may matter.

2.4. Modeling chemical reactions

The temperature T and surface coverages Θ_i describe the state of the catalytic surface. The heterogeneous chemical reactions taking place on this surface are modeled as elementary-like reactions. The reaction source terms \dot{s}_i of gas-phase and surface species are defined by the following expression (Kee et al., 2003):

$$\dot{s}_i = \sum_{k=1}^{K_s} (v''_{ik} - v'_{ik}) k_k \prod_{j=1}^{N_g + N_s} c_j^{v_{jk}}, \quad i = 1, \dots, N_g + N_s \quad (39)$$

Here, K_s is the number of elementary reactions, v''_{ik} (products) and v'_{ik} (reactants) are the stoichiometric coefficients, N_s is the number of surface species and c_j is the molar concentration of species j (in mol/m²) calculated from the product of the surface coverage Θ_i and the surface site density Γ . The rate coefficients k_k are defined as a function of the temperature by means of a modified Arrhenius expression:

$$k_k = A_k T^{\beta_k} \exp\left[-\frac{E_{a_k}}{RT}\right] \prod_{i=1}^{N_s} \Theta_i^{\mu_{ik}} \exp\left[\frac{\varepsilon_{ik} \Theta_i}{RT}\right] \quad (40)$$

The variables μ_{ik} and ε_{ik} are introduced in order to account for the coverage dependence of the reaction rates. Adsorption reactions are described by initial sticking coefficients S_i^0 .

$$k_k^{ads} = S_i^0 \frac{1}{\Gamma \xi} \sqrt{\frac{RT}{2\pi W_i}} \quad (41)$$

The variable S_i^0 represents the adsorption probability at vanishing coverage. The steady-state reactive flow modeled here implies time-independent surface coverages at a given location in the washcoat:

$$\frac{\partial \Theta_i}{\partial t} = \frac{\dot{s}_i}{\Gamma} = 0, \quad i = N_g + 1, \dots, N_g + N_s \quad (42)$$

2.5. Chemical reaction system

The surface reaction mechanism used here is taken from Koop and Deutschmann (2009) and given in the supplementary material. The mechanism is an extension of a multi-step surface reaction mechanism for the description of emission reduction by Rh and Pt catalysts in a three-way converter developed by Chatterjee et al. (2001). The mechanism consists of 11 gas-phase species, 22 surface species and 74 reactions considering dissociative adsorption of CH₄, O₂, and H₂, non-dissociative adsorption of NO, NO₂, N₂O, CO, CO₂, C₃H₆, H₂O and desorption of all species except CH₄.

The applied mechanism consists of mostly reversible reactions describing

- decomposition of hydrocarbons through abstraction of hydrogen atoms;
- oxidation of carbon monoxide to carbon dioxide;
- formation of water via an adsorbed hydroxyl species;
- conversion of nitrogen oxides.

Combustion engine exhaust gases contain more than 100 different hydrocarbon species. In the applied mechanism, C₃H₆ and CH₄ are used as representative species. Propylene takes the impact of reactive hydrocarbons like olefins and aromatic hydrocarbons into account, whereas methane stands for the less reactive hydrocarbons such as alkanes. In the current study, the irreversible adsorption of methane (Reaction 5) does not play any role since this species is not present in the gas-mixture entering the catalyst. The C₃H₆ oxidation proceeds along two reaction paths. The first one comprises adsorption and abstraction of an H-atom leading to the formation of C₃H₅(S) and subsequent cracking of the C–C bonds and oxidation to CO and CO₂. The second path models the dissociative adsorption of C₃H₆, the separated H-Atom reacts with oxygen to a hydroxyl species. The further progress of the reaction is given as a global reaction (Reaction 36). The CO conversion to CO₂ is considered by introducing a Langmuir–Hinshelwood reaction step. A combined Langmuir–Hinshelwood and Eley–Rideal reaction scheme is applied to describe the NO oxidation. Equilibrium calculations show that under lean operating conditions at about 350 °C the NO conversion to NO₂ is thermodynamically restricted.

Because of the lean-phase operating conditions, the reactions involving H₂ and N₂O play no significant role in our simulations. In the current study, homogeneous gas-phase reactions can be neglected due to the low temperatures.

2.6. Model implementation and used software

The plug-flow and boundary-layer models discussed here are based on the DETCHEM software (Tischer et al., 2001; Deutschmann et al., 2008; Tischer and Deutschmann, 2005). This program package applies detailed models for the description of chemical reactions and transport processes in various reactor types. Its core is a library of subroutines to calculate chemical source terms and species thermodynamic and transport parameters. The differential–algebraic equations in DETCHEM are solved by means of the semi-implicit extrapolation DAE-solver LIMEX (Deuflhardt et al., 1987). The plug-flow case is simulated with DETCHEM^{PLUG} and the boundary-layer case with DETCHEM^{CHANNEL}. Both applications assume time-independent laminar operating conditions. The boundary-layer equations are implemented in DETCHEM^{CHANNEL} by means of a method of lines and a finite volume approach is applied to discretize the radial derivatives. The reaction–diffusion equations are solved in

DETCHEM by means of finite difference method with non-equidistant discretization scheme.

The boundary-layer calculations here were carried out with 15 radial mesh points. The LIMEX solver applied in DETCHEM^{CHANNEL} automatically determined the axial step size. The smallest axial steps were computed near the channel inlet, where the highest gradients are observed. Each calculation took roughly 200–500 axial steps for the whole channel length of 20 cm. The only exception was the simulation at 350 °C with the reaction–diffusion washcoat model which turned out to be very stiff, and a maximal step size of 0.0005 m had to be defined. This calculation took about 800 axial steps. The washcoat was resolved with 25 radial points, whereas the mesh was refined near the gas-phase/washcoat interface.

The plug-flow equations are discretized only in axial direction and the LIMEX solver automatically chooses the step size. The step sizes are concentrated near the channel inlet. The calculations considering infinitely fast mass-transport within the washcoat and effectiveness factor approach took about 200–450 steps and these with the reaction–diffusion washcoat model about 90 steps. The washcoat discretization scheme, similarly to the boundary-layer case, consists of 25 non-equidistant mesh points.

The complete Navier–Stokes 2D- and 3D-models are simulated with FLUENT v.6.2.16 (Fluent), whereas DETCHEM user-defined functions (UDFs) provide the chemical source terms (Deutschmann et al., 2008). In the case of channels with mass-transport limitation within the washcoat, the equivalent diffusion coefficients $D_{eff,i}$ are calculated in FLUENT by means of UDFs. The chemical source term $F_{cat/geo} W_i \dot{s}_i$ is also computed through user defined functions.

The porous media model implemented in FLUENT offers two velocity options: superficial and physical velocity. Both velocity formulations can be correlated with each other through the porosity ε :

$$\mathbf{v}_{\text{superficial}} = \varepsilon \cdot \mathbf{v}_{\text{physical}} \quad (43)$$

The default superficial velocity is based on the volumetric flow rate. This approach postulates that the velocity values within and outside the porous region remain the same, i.e. the increase in velocity throughout the porous region is neglected. The expected velocity increase can be taken into account by resolving the more accurate physical (true) velocity throughout the flowfield. However, the continuity of the velocity vectors across the porous medium interface is not preserved leading to considerably lower conversions than with the superficial velocity approach. For this reason, all FLUENT calculations were carried out with the superficial velocity option.

All three-dimensional Navier–Stokes models were meshed with hexahedral finite volumes. In the cases of infinitely fast diffusion within the washcoat and of effectiveness factor calculations, a quarter of the channel cross-section was modeled. The channel with square cross-section was meshed with totally 9000 elements—90 in axial direction \times 100 per cross-section. A mesh with totally 7830 elements was applied to simulate the channel with rounded corners—90 in axial direction \times 87 per cross-section. The calculations, where the washcoat was additionally modeled using FLUENT's porous media option, were the most time-consuming ones and therefore only an eighth of the cross-section was modeled. Here, the channel square cross-section was meshed with totally 47680 elements—80 in axial direction \times 596 per cross-section, whereas 480 elements were for the porous media and 116 for the gas-phase. The numerical model of the square channel with filleted corners consists of 46800 elements—80 in axial direction \times 585 per cross-section (452 porous media and 133 gas-phase elements).

All two-dimensional Navier–Stokes models were discretized with rectangular finite volume elements. For the simple cases (with instantaneous mass-transfer within the washcoat and with the effectiveness factor approach), a mesh of 1616 elements was used—101 in axial and 16 in radial direction. The models, where FLUENT's porous media model is also applied, were meshed with 6161 elements—101 in axial \times 61 in radial direction, from which 35 were porous media and 26 gas-phase elements. Refining of the mesh did not lead to significantly different results.

The 2D- and 3D-Navier–Stokes models were meshed in a way that finer volume elements were placed in the regions expected to have the highest gradients of the velocity and species concentrations. In radial direction, the mesh is concentrated near the wall (or gas-phase/washcoat interface), whereas along the channel the mesh is refined near the channel inlet. In the case of washcoat modeling, a very fine mesh is required in the washcoat near the gas-phase/washcoat interface in order to resolve the high species concentrations gradients. Fulfilling this requirement is a crucial point for the convergence of the numerical solution. As already mentioned, the solution of the Navier–Stokes equations is very computationally expensive, therefore only the first 4 cm of the channel were simulated in FLUENT. The inlet boundary conditions were used as an initial solution guess for the FLUENT simulations, only the 3D calculations with porous media at 350 °C had to be initialized with the solutions from the simulations at 250 °C—the reason for this were the convergence difficulties and long computational time resulting from the inlet boundary conditions initial guess.

3. Results and discussion

3.1. Cases studied

Experimental data from Schmeißer et al. (2007) were used to illustrate the general applicability of the models evaluated. In their experiment, an isothermal flat bed reactor was used consisting of two parallel metal plates. Eight electric heaters separately controlled are incorporated in each of the plates. The bottom plate contains a longitudinal slot, where six slices of single rows of parallel channels cut from a real monolithic converter are placed. Each slice is 4 cm in length and 3 cm in width. The height of 1.43 mm corresponds to the size of the monolithic channels. The first one is inert and responsible for the flow formation and for the gas-mixture preheating. The next five are catalytic active. Thus, the total catalyst length amounts to 20 cm. Every slice is connected to the reactor plates through thin sheets of carbon. The large contact area between monolithic slices and reactor as well as the good heat-conducting properties of carbon guarantee isothermal operating conditions in the catalyst. The small gas channels on the side of the bottom reactor plate enable gas composition analysis at different positions along the slot.

The experimental data used here for comparison were carried out with a synthetic gas-mixture. In order to reproduce a realistic exhaust gas-mixture, various gas flows containing single species were pre-mixed in a flow regulator. The gas-mixture contains CO, CO₂, C₃H₆, H₂O, NO and N₂ as bulk species. Table 1 shows the mixture composition of the applied synthetic gas-mixture.

Table 1
Synthetic gas composition used for the experiments (Schmeißer et al., 2007).

H ₂ O (%)	C ₃ H ₆ (ppm)	CO (%)	CO ₂ (%)	NO (ppm)	NO ₂ (ppm)	O ₂ (%)
10	60	0.04	7	200	40	12

Propylene (C₃H₆) represents the unburnt hydrocarbons. The operating conditions are lean, the O₂-concentration being 12 vol%.

The reactor was operated at atmospheric pressure. Here we use their measurements for two temperatures, 250 and 350 °C, at steady-state conditions. The gas-mixture was fed into the reactor with a constant flow rate corresponding to a gas hourly space velocity (GHSV) of 40 000 h⁻¹.

3.2. Input data

The inlet conditions of the simulation were derived from the experimental conditions. For 250 and 350 °C, the given space velocity corresponds to uniform inlet velocities of 8 and 9.53 m/s and kinematic viscosities of 4×10^{-5} and 5.4×10^{-5} m²/s. The channel diameter is 1 mm. This leads to Reynolds numbers of 201 (250 °C) and 177 (350 °C). Hence, the impact of turbulence, which may exist in front of the channel entrance, is negligible, because even for turbulent inflow fast laminarization can be assumed. An over the cross-section uniform inlet velocity profile is used at the entrance. The establishment of the parabolic velocity profile within the first millimeters of the reactor then mimics the laminarization of the flow field.

In the case of simulations with reaction–diffusion washcoat models, catalyst containing porous media of 100 μm thickness surrounding the channel is additionally modeled. Fig. 1 shows all channel structures used in this study. The plug-flow and boundary-layer calculations were carried out for the entire channel length of 20 cm, whereas the complete Navier–Stokes equations were solved for the first 4 cm of the channel only, for computational reasons. Canu and Vecchi (2002) reported negligible differences between the conversion along segmented and continuous channels. Accordingly, the segmented channels of the experiment were modeled by a single continuous channel in the present study. It should be noted that the experimental data are not used for a detailed evaluation of the accuracy of one or the other mass transfer model applied. The experimental data shall only illustrate that the simulation results in general have practical relevance and agree with experimental data.

In order to compare the cylindrical 2D channel with the 3D rectangular channels, two constraints have to be satisfied:

- The channels must have the same cross-section: $A_{2D} = A_{3D}$. Thus, the mass flow through the channels will be equal. A circular cross-section with $d = 1$ mm corresponds to a square channel with dimension of 0.886 mm and to a filleted square channel with dimension of 0.905 mm and corner rounding radius of 0.2 mm.
- The channels must have the same catalyst loading: $F_{cat/geo,2D}P_{2D} = F_{cat/geo,3D}P_{3D}$, where P is the perimeter of the particular cross-section. The $F_{cat/geo}$ value for all our simulations with cylindrical channel geometry was determined by chemisorption measurements to be 25 (Koop, 2008). The $F_{cat/geo}$ values for the square channels without and with rounded corners amount to 22.1 and 23.9, respectively.

This assumption guarantees comparability of the differences in the conversion due to transport limitations inside the washcoat. If the limitations were mainly caused by the interface

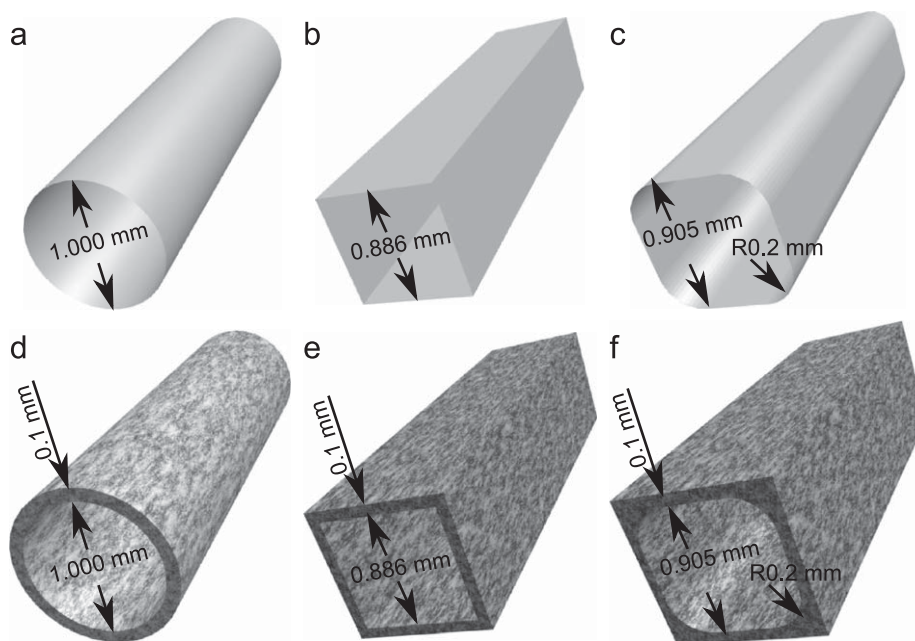


Fig. 1. The analyzed channel geometries: a–c channels with instantaneous diffusion and effectiveness factor washcoat models; d–f channels with reaction–diffusion washcoat model.

gas-phase—washcoat, channels with the same hydraulic diameter must be chosen as constraint. However, here we focus on the influence of the washcoat model.

The washcoat porosity ε was measured to be 40%. According to Kočí et al. (2006), the washcoat particle diameter d_m for a typical automotive monolithic converter is in the order of $1 \mu\text{m}$. Substituting these values in Eqs. (28) and (29), we obtain $\alpha = 1.2 \times 10^{-15} \text{m}^2$ and $C_2 = 3.3 \times 10^7 \text{m}^{-1}$. The computed permeability corresponds to a viscous resistance of $1/\alpha = 8.4 \times 10^{14} \text{m}^{-2}$. In FLUENT, the use of these (large) values led to convergence difficulties. Therefore, we had to gradually lower both the inertial and viscous resistance values until getting a converged solution with $1/\alpha = 4.0 \times 10^{10} \text{m}^{-2}$ and $C_2 = 2.0 \times 10^4 \text{m}^{-1}$. Based on these lower values, the FLUENT simulation do not show any significance of convective mass transport inside the washcoat, which justifies the underestimation of those two factors, because larger values would have suppressed convection even more. The washcoat pore diameter $d_p = 10 \text{nm}$ was determined by BET measurements. This value is in good agreement with the meso- and micro-pore diameters in the range 1–10 nm reported by Kočí et al. (2006). The tortuosity usually lies in the range of 3–4. For our simulations, we used $\tau = 3$.

3.3. Comparison of the 1D, 2D, and 3D models

3.3.1. Channel with infinitely fast mass-transport within the washcoat

In order to compare the species concentration profiles along the channel length provided by the 2D and 3D models with those of the plug-flow models and with experimental results, averaged mole concentrations are introduced. For a certain cross-section the averaged molar concentration \bar{X}_i of the i th species can be expressed as:

$$\bar{X}_i = \frac{\bar{Y}_i W}{W_i} \quad (44)$$

Here, Eq. (21) is used to compute the averaged mass fraction \bar{Y}_i of the species. Fig. 2 shows the comparison of the one dimensional

plug-flow models with and without MTC and the two dimensional boundary-layer and Navier–Stokes models for the case with instantaneous washcoat diffusion at 250°C . The molar concentrations of the species of interest are given in ppm. All calculations show that downstream of $z \approx 16 \text{cm}$ of the channel there are no significant changes in the major species concentrations. The four models also predict the same concentrations at the outlet of the catalyst— C_3H_6 vanishes, the NO concentration amounts to 14 ppm and NO_2 to 225 ppm. As can be expected, the simple plug-flow model overpredicts the conversion of C_3H_6 , NO, and the formation of NO_2 compared to all other solutions due to the missing mass-transport limitation in radial direction. According to this model, C_3H_6 is consumed within the first centimeter of the reactor whereas the remaining models predict complete conversion at $z \approx 6 \text{cm}$. The detailed Navier–Stokes model, where only the first 4 cm of the channel were modeled, is in good agreement with the boundary-layer model. The plug-flow model with MTC represents substantial improvement of the simple plug-flow model, since its species profiles lie close to these of the Navier–Stokes and boundary-layer models.

The comparison of the four models at 350°C shows a similar trend. The 2D boundary-layer and 2D Navier–Stokes contour plots of the C_3H_6 , NO and NO_2 concentrations at 250°C are compared in Fig. 3. They are essentially indistinguishable, i.e. the impact of axial diffusion is negligible. The radial concentration gradients, shown on the figure, point at the importance of radial diffusion limitation when modeling reactive flows. The same conclusion is valid for the contour plot comparison at 350°C .

The axial profiles computed by the two- and three-dimensional Navier–Stokes models (averaged over the cross-section) are practically identical having a maximal differences of 1–2 ppm.

A comparison of the surface coverage profiles of the species O(S), CO(S), and NO(S) at 250°C is shown in Fig. 4. These three species as well as OH(S) and Pt(S) belong to the species with the largest coverage along the catalyst. The coverages of species such as $\text{CO}_2(\text{S})$, $\text{C}_3\text{H}_6(\text{S})$, $\text{H}_2\text{O}(\text{S})$, N(S), and $\text{NO}_2(\text{S})$ are below 0.1% and will not be discussed here. As expected, the catalyst's wall is mainly covered with oxygen ($\sim 97.4\%$ at the outlet) as a result

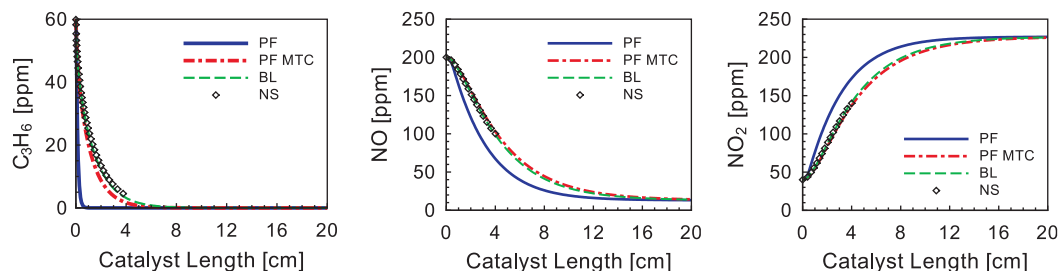


Fig. 2. Comparison of the plug-flow (PF), plug-flow with mass transfer coefficients (PF MTC), boundary-layer (BL) and 2D Navier–Stokes (NS) solutions for a channel with instantaneous washcoat diffusion at 250 °C.

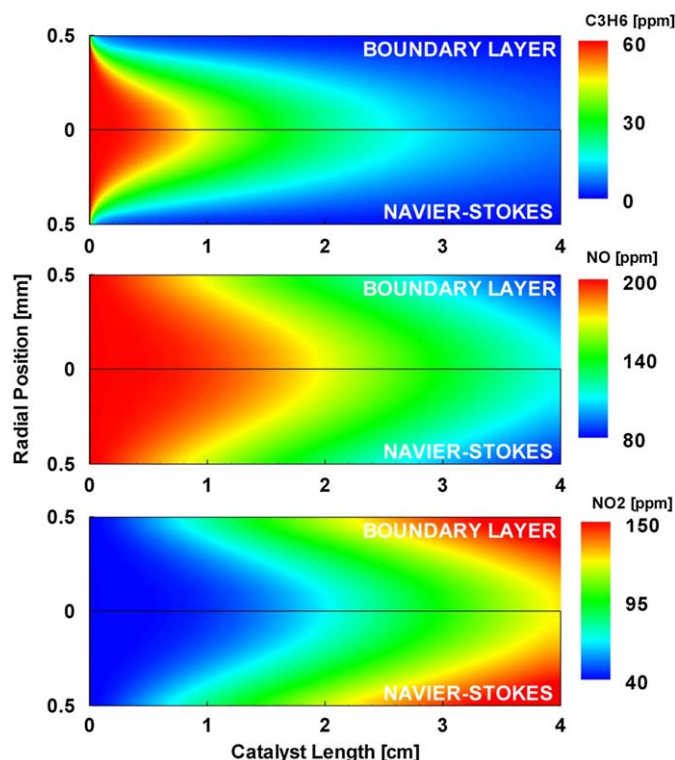


Fig. 3. Contour plots of the mean species profiles computed with the boundary-layer (BL) and 2D Navier–Stokes (NS) models for a channel with instantaneous washcoat diffusion at 250 °C.

of the oxygen excess at lean operating conditions. $\text{CO}(\text{S})$ is completely oxidized to $\text{CO}_2(\text{S})$ within the first 5 cm of the channel. Initially, the number of active sites covered with NO increases, reaching a maximum at $z \approx 1$ cm. Up to this point, the adsorption of NO predominates over the formation of $\text{N}(\text{S})$ and $\text{NO}_2(\text{S})$ from $\text{NO}(\text{S})$ on the catalytic wall. Subsequently, the $\text{NO}(\text{S})$ coverage along the channel decreases reaching a value of 0.1% at the outlet. The coverages of $\text{OH}(\text{S})$ and the vacant sites $\text{Pt}(\text{s})$ increase in axial direction until they reach a maximum of 1.2% at $z \approx 10$ cm, remaining constant further downstream. The impact of the mass transport in the gas-phase on the surface chemistry is revealed in these curves. Due to the instantaneous radial diffusion, the chemical reactions with the simple plug-flow model are accomplished in a shorter channel section than with the other models. The plug-flow model with MTC, as well as the boundary-layer and Navier–Stokes, models behave essentially alike. At 350 °C, the differences in the coverages predicted by the simple-plug-flow model on one hand and the remaining models on the other hand diminish significantly.

3.3.2. Effectiveness factor washcoat model

As recognized by comparison of Figs. 2 and 5, the use of an effectiveness factor washcoat model with NO as representative species has a slight impact on the consumption of C_3H_6 . According to the plug-flow model, it is completed within the first 2 cm and the three other models (plug-flow with MTC, boundary-layer, Navier–Stokes) within the first 7–8 cm of the catalytic channel. However, the effectiveness factor approach has a much stronger impact on the conversion of NO and NO_2 . Both species do not reach constant concentrations at 250 °C and the plug-flow model overpredicts the conversion of NO and formation of NO_2 , even at the outlet. Here, the differences concerning the NO and NO_2 profiles predicted by the simple plug-flow model and the other models are smaller compared to the simulations without mass-transport limitation within the washcoat. Without diffusion limitation, the maximum difference amounts to 30–35 ppm for both investigated temperatures. Applying the effectiveness factor approach, the difference does not exceed 12–13 ppm at 250 °C. At 350 °C, the maximal difference amounts to 7–8 ppm and the partial equilibrium between NO and NO_2 is reached at $z \approx 16$ cm. As expected, they coincide with the outlet concentrations from the calculation without mass-transport limitation within the washcoat. For the case studied here, we can conclude that mass-transfer limitation is rather caused by diffusion in the washcoat than radial diffusion in bulk flow.

The species profiles predicted by the 2D and 3D Navier–Stokes models are in good agreement, figures illustrating the results of those computations and many others can be found in the supplementary material. It is noted that the 2D solution for the three species of interest slightly underpredicts the two 3D solutions at 250 °C. However, the difference does not exceed 3 ppm and can be therefore neglected; they are even smaller at 350 °C.

Similar to the calculation without mass-transport limitation within the washcoat, the coverages predicted by the simple plug-flow model considerably differ from these of the other three models. The effectiveness factor washcoat model affects the profiles of $\text{O}(\text{S})$ and $\text{NO}(\text{S})$ by “stretching out” the curves from the simulation without washcoat diffusion limitation (Fig. 4). Both species do not reach steady-state down to the outlet of the catalyst.

3.3.3. Reaction–diffusion washcoat model

The differences between the simple plug-flow model and the remaining three models significantly decrease when coupling them with a reaction–diffusion model. The reason for this is the diffusion limitation in the porous media which prevails over the transport limitation in the gas-phase. For the species of interest, these differences do not exceed 5–6 ppm at 250 °C, Fig. 6. At 350 °C, the maximal difference reaches nearly 10 ppm for C_3H_6

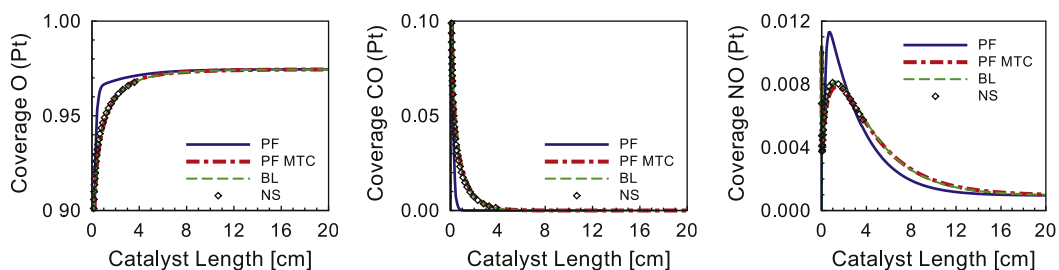


Fig. 4. Comparison of main surface species profiles provided by the plug-flow (PF), plug-flow with mass transfer coefficients (PF MTC), boundary-layer (BL) and 2D Navier–Stokes (NS) solutions for a channel with instantaneous washcoat diffusion at 250 °C.

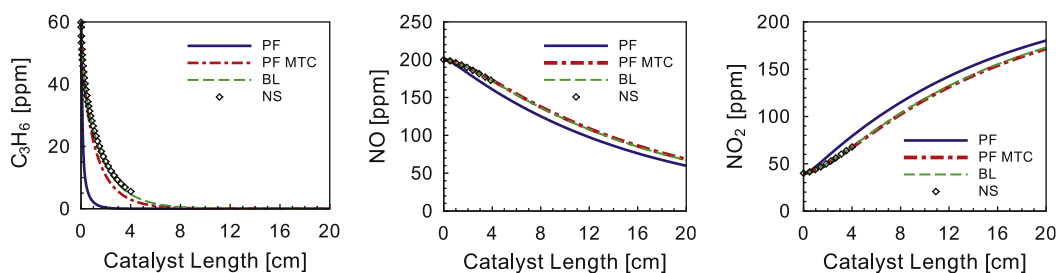


Fig. 5. Comparison of the plug-flow (PF), plug-flow with mass transfer coefficients (PF MTC), boundary-layer (BL), and 2D Navier–Stokes (NS) solutions for a channel with mass-transport limitation within the washcoat at 250 °C (effectiveness factor approach).

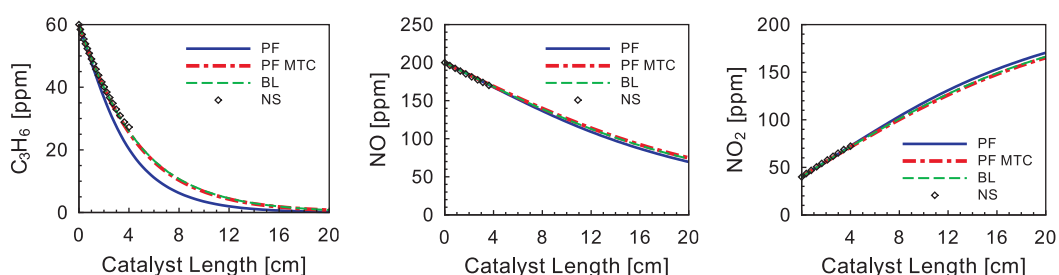


Fig. 6. Comparison of the plug-flow (PF), plug-flow with mass transfer coefficients (PF MTC), boundary-layer (BL), and 2D Navier–Stokes (NS) solutions for a channel with mass-transport limitation within the washcoat at 250 °C (reaction–diffusion washcoat model).

and amounts to about 5 ppm for NO and NO₂. The diffusion inside the porous media considerably slows down the formation/depletion of the gas-mixture species. C₃H₆ is consumed completely just at the channel outlet at 250 °C and at $z \approx 12$ cm at 350 °C, while the NO and NO₂ concentrations change along the whole channel at both temperatures.

The species profiles provided by the circular and both square channels are in good agreement. Similar to the calculations without mass transport within the washcoat and with effectiveness factor washcoat model, the averaged concentrations of the major species practically coincide, with differences ranging up to 1 ppm. The only exception is the C₃H₆ concentration at 350 °C, the circular channel approximation increasingly overpredicts the conversion of propylene in contrast to the slightly underpredicting simpler washcoat models. At the outlet of the converter the difference from both 3D models amounts to 4 ppm.

The solutions for the surface species Pt(S), O(S), CO(S) and NO(S) computed with the 1D reaction–diffusion model of DETCHEM (coupled with the boundary-layer model) and with the 2D reaction–diffusion model implemented in FLUENT (Navier–Stokes model) provide identical 2D contour plots (shown in the supplementary material), in which the gradients in radial direction are considerably larger than in axial direction. The number of vacant sites increases in radial direction, reaching a constant

coverage value of 1.2% within the first 15 μm of the washcoat. This value corresponds to the maximum Pt(S) coverage reported in Section 3.3.1 for calculations with infinitely fast diffusion within the washcoat. Initially, the NO(S) coverage increases in radial direction and subsequently decreases, reaching the constant value of 0.1% reported in Section 3.3.1. The surface species profiles in radial direction are essentially identical with the profiles in axial direction discussed in Section 3.3.1. Here, the length scale of the problem is determined by the diffusion rate inside the washcoat, whereas in the case of instantaneous diffusion within the washcoat it is determined by the convection in the gas-phase. The O(S) and CO(S) profiles are practically uniform—gradients are observed only at the gas-phase/washcoat interface.

Fig. 7 reveals the radial concentration profiles of the major gas-phase species at $z=1$ cm and $T=250$ °C. The grey area at the right-hand side of each diagram identifies the washcoat zone. The boundary-layer and Navier–Stokes solutions are in good agreement in the gas-phase as well as in the porous media: the maximal differences, detected in the washcoat near the gas-phase/washcoat interface, do not exceed 3–4 ppm. As can be expected, the highest concentration gradients also occur there. Propylene is consumed within the first 20 μm of the washcoat, whereas the conversion of NO and formation of NO₂ are not completed up to the washcoat/wall boundary.

At $T=350\text{ }^{\circ}\text{C}$, the concentration gradients in the near-interface porous media region are higher and the maximal differences between both solutions lie in the range of 6–7 ppm for NO and NO_2 . In regions with low gradients the differences diminish: in the gas-phase, they do not exceed 2 ppm all three species at both temperatures.

3.4. Comparison of the washcoat models with the experimental data

Due to its computational complexity, the detailed Navier–Stokes model was applied only for the first 4 cm section part of the reactor. However, it was shown in the previous section that the boundary-layer and the Navier–Stokes calculations are essentially alike in the simulated cases with and without mass-transport limitation within the washcoat. On that account, the results from the boundary-layer simulation were chosen for the comparison with the experimental data. The comparison of the calculations with instantaneous washcoat diffusion and with washcoat limitation (effectiveness factor approach and reaction–diffusion model) and experiment is presented in Fig. 8 for $T=250\text{ }^{\circ}\text{C}$ and in Fig. 9 for $T=350\text{ }^{\circ}\text{C}$. The experiments show a slight inhibition of the NO oxidation and NO_2 formation in the first 4 cm of the channel caused by CO and C_3H_6 . Both washcoat simulations at $250\text{ }^{\circ}\text{C}$ also indicate this inhibition—in the first 1 cm of the reactor

length the NO and NO_2 concentrations remain nearly constant. In both figures can be seen that the effectiveness factor washcoat simulation has a negligible impact on the consumption of propylene compared to the calculation with instantaneous washcoat diffusion. Both C_3H_6 -curves are close to each other and show a good agreement with the experimentally derived data. On the other hand, the C_3H_6 -conversion is underpredicted by the reaction–diffusion model, there is a significant deviance from the experiment. The calculation without mass-transport limitation within the washcoat predicts substantially faster conversion of NO and formation of NO_2 than the experimental data. At $250\text{ }^{\circ}\text{C}$, both washcoat models predict identical profiles for these two species, they agree well with the measured concentrations. At the higher temperature they differ from each other with the reaction–diffusion solution lying closer to the experiment. All three models overpredict the experimental NO and NO_2 profiles.

There are two significant conclusions drawn from the comparison of experimental and computed data. (1) The effectiveness factor model is not applicable for all operating conditions. Gradients in species concentration and surface coverage within the washcoat have an effect on the overall conversion. The effectiveness factor shall be used with care only. An improvement of the effectiveness factor model may be achieved if the representative species for computing the Thiele module is adapted to the local concentrations along channel. (2) The

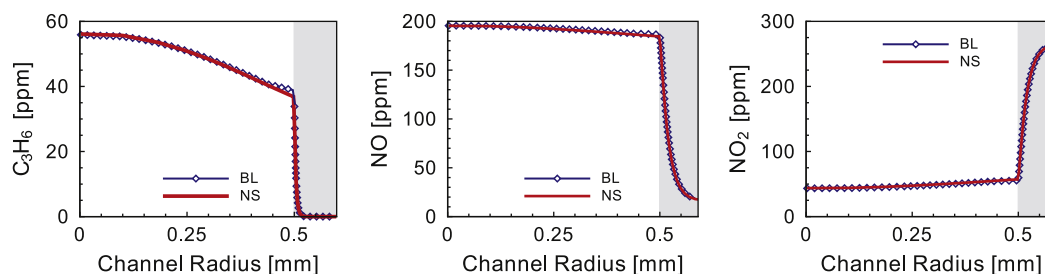


Fig. 7. Comparison between the boundary-layer (BL) and 2D and Navier–Stokes (NS) solutions in radial direction for a channel with mass-transport limitation within the washcoat at $250\text{ }^{\circ}\text{C}$ at $z \approx 1\text{ cm}$.

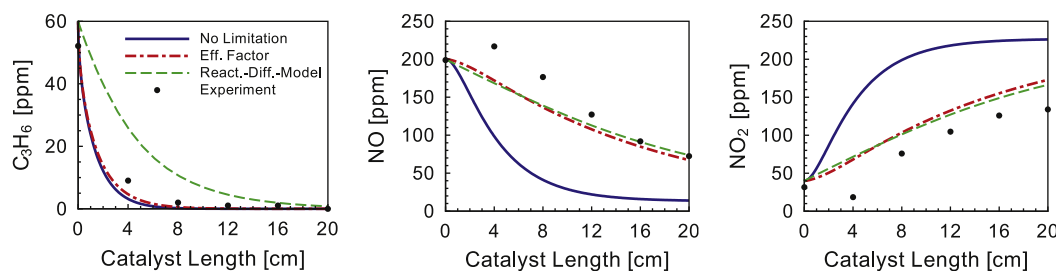


Fig. 8. Comparison of the boundary-layer solutions without (no limitation) and with washcoat diffusion limitation (eff. factor approach and reaction–diffusion model) and experiment at $250\text{ }^{\circ}\text{C}$.

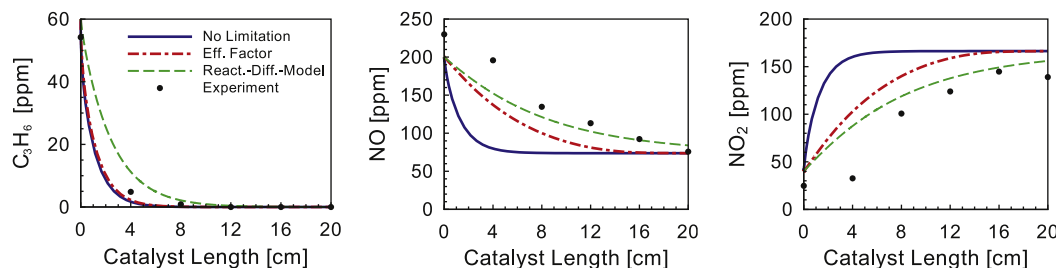


Fig. 9. Comparison of the boundary-layer solutions without (no limitation) and with washcoat diffusion limitation (eff. factor approach and reaction–diffusion model) and experiment at $350\text{ }^{\circ}\text{C}$.

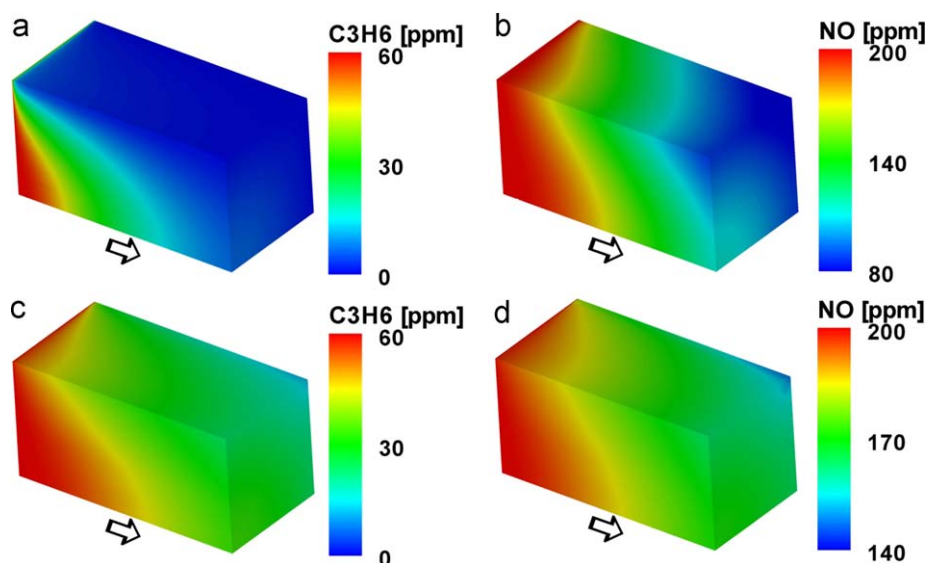


Fig. 10. Comparison of the concentration profiles for a 3D-channel with square cross-section at 250 °C: (a) and (b) with instantaneous washcoat diffusion; (c) and (d) with mass-transport limitation within the washcoat (3D reaction diffusion model). The arrows at the symmetry axes show the main flow direction.

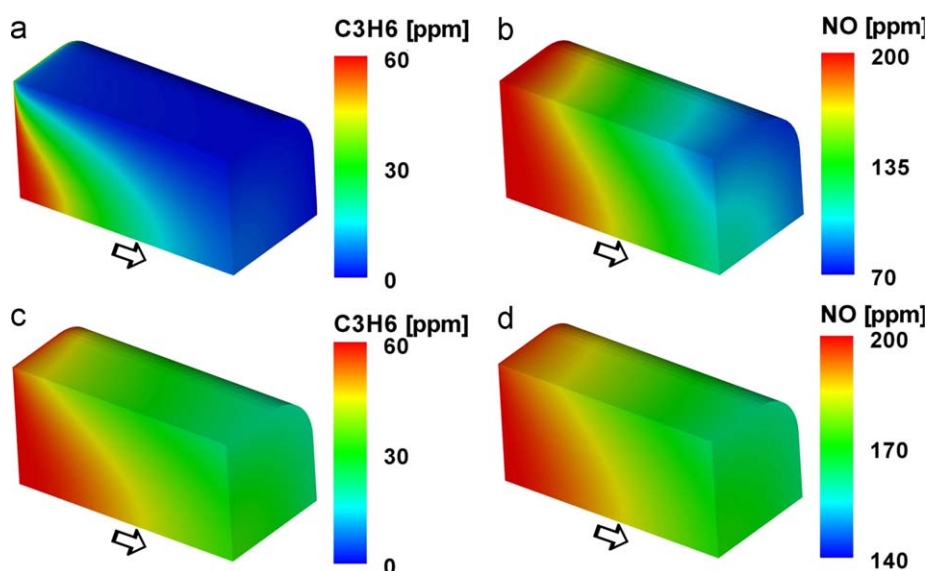


Fig. 11. Comparison of the concentration profiles for a 3D-channel with filleted corners at 250 °C (a) and (b) with instantaneous washcoat diffusion; (c) and (d) with mass-transport limitation within the washcoat (3D reaction diffusion model). The arrows at the symmetry axes show the main flow direction.

mechanism (Koop and Deutschmann, 2009) applied was developed using transport models that included an effectiveness factor approach and NO of representative species. Both of these assumptions—we learn by the present study—led to slight oversimplifications concerning mass transfer in the washcoat. Hence, the mechanism does not fully represent the micro (intrinsic) kinetics; there is still—even though small—a mass transfer effect included in the kinetic data.

3.5. Three-dimensional transport effects

The comparisons of the averaged major species concentrations in axial direction provided by the 2D and 3D models were presented in Section 3.3. The 2D solution and both 3D solutions were shown to be in good agreement in all three cases: instantaneous washcoat diffusion, simplified washcoat model (effectiveness factor approach), and detailed reaction–diffusion

washcoat model. Fig. 10 compares the C₃H₆ and NO profiles for a quarter of the channel with square cross-section at 250 °C. The contour plots (a) and (b) illustrate the solution for a channel with instantaneous washcoat diffusion, whereas plots (c) and (d) show the solution with 3D reaction–diffusion model. For the purpose of clarity, the concentration profiles in the washcoat are not shown in (c) and (d), only the gas-phase profiles are shown. A similar comparison for the square channel with rounded corners is presented in Fig. 11. Those simulations reveal that the highest conversion of C₃H₆ and NO occurs at the channel corner. This is expected, since the conversion from both mutually perpendicular boundaries is superimposed in this region. The conversion decreases with increasing distance from the corners, reaching a minimum in the middle of each side. This effect is weaker in the case of a channel with rounded corners, since its geometrical structure is more similar to the circular geometry, where the effect vanishes.

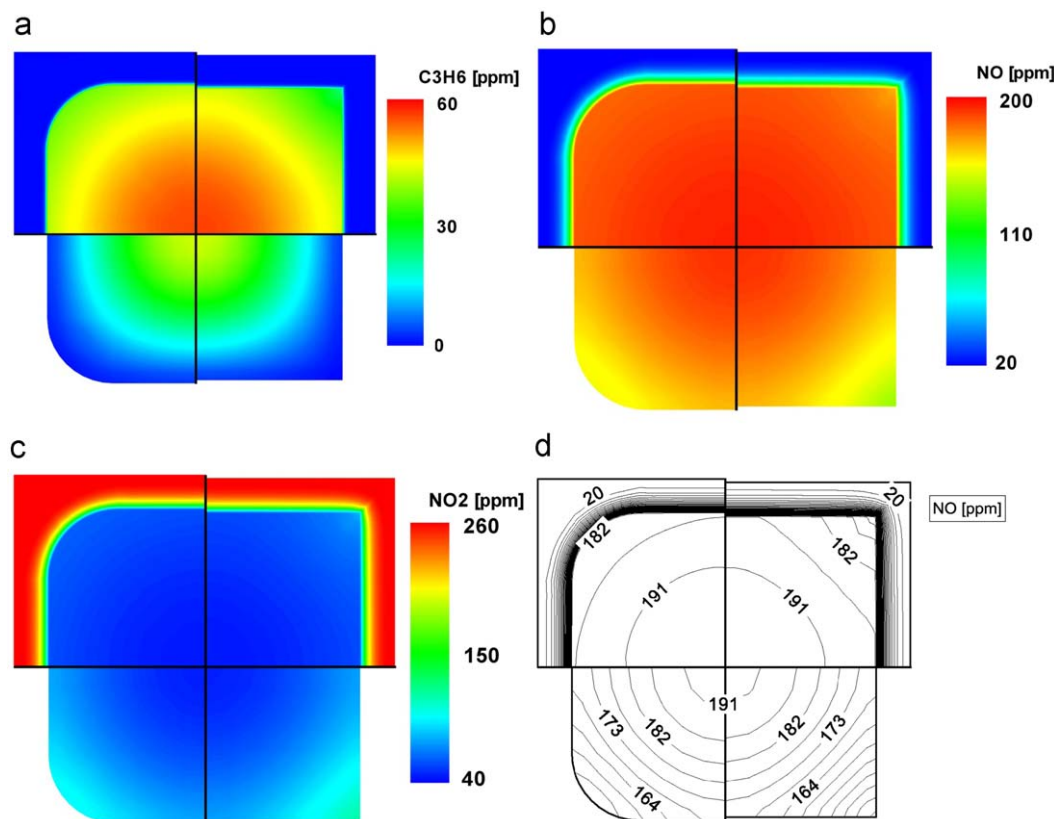


Fig. 12. Comparison of the concentration profiles for the various 3D channel geometries with and without mass-transport limitation within the washcoat at 250 °C and $z=1$ cm: (a) C_3H_6 concentration; (b) NO concentration; (c) NO_2 concentration; (d) NO concentration, contour lines. The perpendicular black lines represent the planes of symmetry.

The effect described above can be also seen in Fig. 12. The figure shows channel cross-sections with the corresponding C_3H_6 , NO, and NO_2 profiles at $z=1$ cm for the following cases:

- channel with rounded corners and reaction–diffusion washcoat model (top left, Fig. 1f);
- channel with rounded corners and instantaneous washcoat diffusion (bottom left, Fig. 1e);
- channel with square cross-section and reaction–diffusion washcoat model (top right, Fig. 1c);
- channel with square cross-section and instantaneous washcoat diffusion (bottom right, Fig. 1b).

Here, a quarter of each channel is presented, with both perpendicular black lines marking the planes of symmetry. The corresponding dimensions are given in Fig. 1. Both channels with instantaneous washcoat diffusion behave essentially alike. Near the channel centre, the regions with identical concentration have circular form, Fig. 12d. Approaching the channel corners, the circular contours pass into parallel line segments. In the case of a channel with mass-transport limitation within the washcoat, this transition from circular to linear contours is distinguishable, for the channel with square cross-section corners as well. However, linear contours are not observed by the channel with rounded corners and washcoat mass-transport limitation. This can be explained with the interaction of two factors:

- the geometry of the square channel with rounded corners is closer to the circular geometry compared to the square channel;

- the mass transport limitation in the porous media dominates over the transport limitation in the bulk fluid.

In contrast to the propylene profiles inside the washcoat (Fig. 12a), where the species is consumed within the first few μm of the porous media, NO and NO_2 are converted and formed, respectively, within the 30–40 μm . The regions of the washcoat with identical concentrations lie parallel to the gas-phase/washcoat interface, Fig. 12b–d.

3.6. Comparison of the computational times

CPU time for the computations presented vary by several orders of magnitude, reaching from few seconds for the plug-flow models without washcoat model to several days for 3d Navier–Stokes model with detailed washcoat model. More information can be found in the supplementary material.

4. Conclusions

The current study presents a broad spectrum of numerical models for the simulation of mass transfer in automotive catalytic converters. The chemical conversion on the Pt-catalyst is modeled by a detailed surface reaction mechanism. For the first time to our knowledge, three-dimensional flow field simulations including detailed washcoat and chemistry models are coupled and a comprehensive evaluation of simplified transport models by comparison with this complex model is carried out.

Two one-dimensional, two two-dimensional, and two three-dimensional channel models under isothermal steady-state conditions have been compared with each other. In total, three

channel geometries have been considered—with circular cross-section, square cross-section, and square cross-section with rounded corners. The influence of diffusion within the washcoat is taken into account by introducing a simplified effectiveness factor and a detailed reaction–diffusion porous media model. The simulations have been carried out with the computational tools DETCHEM and FLUENT. The complexity of the models varies from 1D plug-flow model without mass-transport limitation within the washcoat to a 3D Navier–Stokes model with detailed reaction–diffusion model.

The Navier–Stokes models used for 2D and 3D simulations have only few assumptions and provide the most accurate solution. However, they are much more computationally expensive than the simpler models. The boundary-layer approach neglecting axial diffusion is in very good agreement with the Navier–Stokes model and significantly reduces the computational time. The simple plug-flow model ignoring the radial and axial diffusion terms is the most computationally inexpensive but it predicts much faster conversion/formation of the major gas-phase species compared to the remaining models. Mass-transfer coefficients improve the accuracy of the plug-flow solution. However, they have to be used with caution since they are based on empirical correlations.

Diffusion of chemical species in the porous washcoat is revealed to present a largest mass transfer effect than radial diffusion from the bulk fluid to the washcoated wall. The simple effectiveness factor washcoat model is computationally inexpensive, but its universal validity is questionable since it does not affect all species concentration profiles (C_3H_6 in our case). Simulations with detailed reaction–diffusion models are the most computationally expensive but allow discrimination between intrinsic kinetics and mass transfer effects and provide the best agreement with the experimental data. Furthermore, washcoat models reduce the differences in the radial-averaged gas-phase species profiles provided by the various flow models.

The 2D and both 3D Navier–Stokes models basically show no significant difference in species profiles. Hence, 3D reactive channels can be approximated by the less computationally expensive 2D cylindrical channel models.

Summarizing, we can conclude that mass transfer in honeycomb structured automotive catalytic converters at moderate temperatures can be governed by relatively simple flow field models (plug-flow with mass-transfer coefficient and 2d cylindrical boundary layer equations) but require more sophisticated models for the description of diffusion in the washcoat.

It should be noted that these conclusions are drawn for a chemical system with relatively low surface reaction rates due to relatively low temperatures and reactants' concentration. In particular at higher temperature and high reactants' concentrations, e.g. partial and total oxidation of hydrocarbons in noble metal coated monoliths, where also homogeneous gas-phase reactions may occur, model simplifications used here may not be justified anymore. In particular, it can be expected that radial mass transfer in the gaseous bulk phase becomes more important. Simulation for such systems will be discussed in a forthcoming publication.

The computational tools presented allow detailed studies of the behaviour of automotive catalytic converters consisting of monolithic structures. These numerical simulations can help to optimize the shape of the channels/washcoats and the catalyst loading to achieve the conversion needed but keep the amount of catalyst material as small as possible. In the present study, we mainly applied those tools to advise the right choice of transport models for simulation of catalytic converters. In addition to that, these computations can also easily be used to study the effect of spatially inhomogeneous catalyst loading (so-called zone coatings) and the variation of the catalyst loading in time (aging).

Furthermore, the detailed washcoat models may be used to study the impact and interaction of multiple catalysts in the structure.

Notation

A	surface area of the channel cross-section
$A_{2D/3D}$	cross-section area of the channel (2D/3D case)
A_k	pre-exponential factor of the Arrhenius expression
$c_{i,w}$	molar concentration of species i in the washcoat
c_j	molar concentration of species j
$c_{0,i}$	concentration at the gas-phase/washcoat interface
C_2	washcoat inertial resistance
d	channel diameter
d_m	mean washcoat particle diameter
d_p	washcoat pore diameter
$D_{eff,i}$	equivalent Fick coefficient for species i
$D_{knud,i}$	Knudsen diffusion coefficient for species i
$D_{M,i}$	mixture diffusion coefficient for species i
E_{a_k}	activation energy
$F_{cat/geo}$	ratio between catalytic active surface area and geometric surface area
\vec{F}	body forces in x , y and z direction
Gz_i	Graetz number
h_i	mass-transfer coefficient of species i
\vec{J}_i	diffusive mass flux of species i
$\vec{J}_{i,r}^w$	diffusive molar flux of species i in radial direction
k	rate constant
K_s	number of elementary surface reactions
L	channel length
N_g	number of gas-phase species
N_s	number of surface species
p	static pressure
$P_{2D/3D}$	perimeter of the channel (2D/3D case)
r	radial spatial coordinate(1D and 2D case)
$r_{channel}$	channel radius
R	ideal gas constant
Re	Reynolds number
$\dot{S}_{eff,i}$	effective heterogeneous reaction source term for species i (effectiveness factor approach)
\dot{S}_i	heterogeneous reaction source term for species i
\vec{S}	momentum source term
S_i^0	initial sticking coefficient
Sc	Schmidt number
Sh	Sherwood number
t	time
t_w	washcoat thickness
T	temperature
v	radial velocity
\vec{v}	velocity vector
w	axial velocity
\bar{W}	averaged molar mass of the gas-mixture
W_i	molar mass of species i
$x/y/z$	spatial coordinates
\bar{X}_i	averaged mole fraction of species i for a certain cross-section of the channel
Y_i	mass fraction of species i
\bar{Y}_i	averaged mass fraction of species i for a certain cross-section of the channel

Greek letters

α	permeability
β	parameter for temperature dependent rate coefficient

γ	catalyst density (active surface per washcoat volume)
Γ	surface site density
ε	washcoat porosity
ζ_{ik}	parameter for coverage dependent activation energy
η	washcoat effectiveness factor
Θ_i	surface coverages (fraction of surface sites covered by species i)
μ	dynamic viscosity
v_{ik}'' , v_{ik}'	stoichiometric coefficients
ξ	number of occupied adsorption sites of species i
ρ	density
τ	washcoat pore tortuosity
χ_{ik}	parameter for coverage dependent reaction order
$\dot{\omega}_i$	homogeneous reaction source term for species i

Acknowledgements

The authors would like to gratefully thank our former colleague Vinod Janardhanan (now University of Cambridge) and Robert J. Kee (Colorado School of Mines) for many useful discussions. We also owe special thanks to Volker Schmeißer and Gerhard Eigenberger (both at University of Stuttgart) for sharing their experimental data. We acknowledge funding by the German Research Foundation (DFG).

Appendix A. Supplementary material

Supplementary data associated with this article can be found in the online version at doi:10.1016/j.ces.2009.09.034.

References

- Appel, C., Mantzaras, J., Schaeren, R., Bombach, R., Inauen, A., Kaeppli, B., Hemmerling, B., Stampanoni, A., 2002. An experimental and numerical investigation of homogeneous ignition in catalytically stabilized combustion of hydrogen/air mixtures over platinum. *Combustion and Flame* 128, 340–368.
- Baba, N., Oshawa, K., Sugiura, S., 1996. Numerical approach for improving the conversion characteristics of exhaust catalysts under warming-up condition, SAE Technical Paper 962076.
- Canu, P., Vecchi, S., 2002. CFD simulation of reactive flows: catalytic combustion in a monolith. *A.I.Ch.E. Journal* 48 (12), 2921–2935.
- Chatterjee, D., 2001. Detaillierte Modellierung von Abgaskatalysatoren, Dissertation (Ph.D. Thesis), Naturwissenschaftlich—Mathematische Gesamtfakultät der Ruprecht-Karls-Universität Heidelberg.
- Chatterjee, D., Deutschmann, O., Warnatz, J., 2001. Detailed surface mechanism in a three-way catalyst. *Faraday Discussions* 119, 371–384.
- Chatterjee, D., Correa, C., Deutschmann, O., Maier, L., Tischer, S., Warnatz, J., Braun, J., Hauber, T., Többen, H., Windmann, J., Zacke, P., 2002. Three-dimensional simulation of the transient behavior of a three-way catalytic converter, SAE Technical Paper 2002-01-0065.
- Deuffhardt, P., Hairer, E., Zugk, J., 1987. One-step and extrapolation methods for differential–algebraic systems. *Numerische Mathematik* 51, 501–516.
- Deutschmann, O., Schmidt, L.D., 1998. Modelling the partial oxidation of methane in a short contact time reactor. *A.I.Ch.E. Journal* 44, 2465–2476.
- Deutschmann, O., Schwiedernoch, R., Maier, L., Chatterjee, D., 2001. Natural gas conversion in monolithic catalysts: interaction of chemical reactions and transport phenomena. In: Iglesias, E., Spivey, J.J., Fleisch, T.H. (Eds.), *Natural Gas Conversion VI, Studies in Surface Science and Catalysis*, vol. 136. Elsevier, pp. 215–258.
- Deutschmann, O., Tischer, S., Correa, C., Chatterjee, D., Kleditzsch, S., Janardhanan, V.M., 2008. DETCHEM software package, 2.1. ed., <www.detchem.com>, Karlsruhe.
- Fluent Inc., FLUENT user manual 6.2, www.fluent.com, Lebanon, New Hampshire 03766.
- Groppi, G., Tronconi, E., 1997. Theoretical analysis of mass and heat transfer in monolith catalysts with triangular channels. *Chemical Engineering Science* 52, 3521–3526.
- Hayes, R.E., Kolaczkowski, S.T., 1997. *Introduction to Catalytic Combustion*. Gordon and Breach Science Publishers, Amsterdam.
- Hayes, R.E., Liu, B., Moxom, R., Votsmeier, M., 2004. The effect of washcoat geometry on mass transfer in monolith reactors. *Chemical Engineering Science* 59, 3169–3181.
- Holmgren, A., Andersson, B., 1998. Mass transfer in monolith catalysts—CO oxidation experiments and simulations. *Chemical Engineering Science* 53, 2285–2298.
- Jahn, R., Šnita, D., Kubíček, M., Marek, M., 1997. 3-D modeling of monolith reactors. *Catalysis Today* 38, 39–46.
- Kee, R.J., Coltrin, M.E., Glarborg, P., 2003. *Chemically Reacting Flow: Theory and Praxis*. Wiley, Hoboken, New Jersey.
- Kočí, P., Štěpánek, F., Kubíček, M., Marek, M., 2006. Meso-scale modelling of CO oxidation in digitally reconstructed porous Pt/ γ -Al₂O₃ catalyst. *Chemical Engineering Science* 61, 3240–3249.
- Koop, J., 2008. Detaillierte Modellierung der Pt-katalysierten Schadstoffminderung in Abgasen moderner Verbrennungsmotoren, Dissertation (Ph.D. Thesis), Fakultät für Chemieingenieurwesen und Verfahrenstechnik, Universität Karlsruhe (TH).
- Koop, J., Deutschmann, O., 2009. Detailed surface reaction mechanism for Pt-catalysed abatement of automotive exhaust gases. *Applied Catalysis B: Environment* 91, 47–58.
- Leung, D., Hayes, R.E., Kolaczkowski, S.T., 1996. Diffusion limitation effects in the washcoat of a catalytic monolith reactor. *The Canadian Journal of Chemical Engineering* 74, 94–102.
- Maestri, M., Beretta, A., Faravelli, T., Groppi, G., Tronconi, E., Vlachos, D., 2008. Two-dimensional detailed modeling of fuel-rich H₂ combustion over Rh/Al₂O₃ catalyst. *Chemical Engineering Science* 63, 2657–2669.
- Raja, L., Kee, R., Deutschmann, O., Warnatz, J., 2000. A critical evaluation of Navier–Stokes, boundary-layer and plug-flow models of the flow and chemistry in a catalytic-combustion monolith. *Catalysis Today* 59, 47–60.
- Ramanathan, K., Balakotaiah, V., West, D.H., 2004. Geometry effects on ignition in catalytic monoliths. *A.I.Ch.E. Journal* 50, 1493–1508.
- Schlichting, H., 1968. *Boundary-Layer Theory*, sixth ed McGraw-Hill, New York.
- Stutz, M.J., Poulidakos, D., 2007. Optimum washcoat thickness of a monolith reactor for syngas production by partial oxidation of methane. *Chemical Engineering Science* 63, 1761–1770.
- Schmeißer, V., de Riva Pérez, J., Tuttlies, U., Eigenberger, G., 2007. Experimental results concerning the role of Pt, Rh, Ba, Ce and Al₂O₃ on NO_x-storage catalyst. *Topics in Catalysis* 42–43, 15–19.
- Tischer, S., Correa, C., Deutschmann, O., 2001. Transient three-dimensional simulation of a catalytic combustion monolith using detailed models for heterogeneous and homogeneous reactions and transport phenomena. *Catalysis Today* 69, 57–62.
- Tischer, S., Deutschmann, O., Warnatz, J., Windmann, J., Braun, J., Zacke, P., 2003. Impact of the inlet flow distribution on the light-off behavior of a 3-way catalytic converter. SAE Technical Paper 2003-01-0937.
- Tischer, S., Deutschmann, O., 2005. Recent advances in numerical modeling of catalytic monolith reactors. *Catalysis Today* 105, 407–413.
- Tuttlies, U., Schmeißer, V., Eigenberger, G., 2004. A mechanistic simulation model for the NO_x storage catalyst dynamics. *Chemical Engineering Science* 59, 4731–4738.
- Wanker, R., Raupenstrauch, H., Staudinger, G., 2000. A fully distributed model for the simulation of a catalytic combustor. *Chemical Engineering Science* 55, 4709–4718.